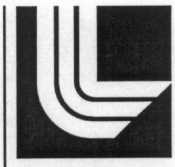

LAWRENCE
LIVERMORE
NATIONAL
LABORATORY

UCRL-JC-152004

Filamentation, Deflection, Scatter, and Crossed Beam Energy Transfer in High Temperature Hohlraums

D.E. Hinkel, L.J. Suter, M.B. Schneider, P.T. Springer, A.B. Langdon, E.A. Williams

September 4, 2003

2003 Third International Conference on Inertial Fusion Sciences and Applications, Monterey, CA, September 7-12, 2003

This work was performed under the auspices of the U.S. Department of Energy by University of California, Lawrence Livermore National Laboratory under Contract W-7405-Eng-48.

Filamentation, deflection, scatter, and crossed beam energy transfer in high temperature hohlraums

D. E. Hinkel, M. B. Schneider, E. A. Williams, A. B. Langdon, L. J. Suter, and P. T. Springer
Lawrence Livermore National Laboratory
P.O. Box 808, Livermore, CA 94550

(Dated: September 4, 2003)

High temperature hohlraums are reduced-scale targets shot at high power. The creation of such hot environments is crucial to material science studies under extreme conditions. A key ingredient in creating hot environments is to successfully couple the laser energy into the target. Maximum coupling is limited in high temperature hohlraums by laser-plasma interactions that occur outside the target (the target fills up on the time scale of the laser pulse).

High temperature hohlraums shot at the Omega laser at the Laboratory for Laser Energetics (Rochester, NY) show reduced energy coupling. Comparison between experiments and radiation-hydrodynamic simulations show that as much as 40% of the incident energy is unaccounted for in the smaller targets. Laser-plasma interaction in such targets occur in a regime of high intensity, high density, and high electron temperature. Novel saturation mechanisms such as Brillouin re-scatter of Raman forward scatter have been predicted to exist in this regime.[1]

The interplay between filamentation/deflection and laser scatter is simulated and analyzed in this regime. Crossed beam energy transfer from the inner to the outer beams[2] will further reduce the drive and these effects are incorporated into the fluid simulations as well. Particle-in-cell simulations of Raman scatter and MPP fluid simulation results will be presented. Initial fluid simulation results show dramatic filamentation, deflection and absorption along the outermost beams of the Omega laser.

I. INTRODUCTION

The creation of hot environments using lasers enables advances in material science studies under high energy density conditions. One manner in which such an environment is formed is by shining laser light into the interior of a high-Z enclosure. The laser light is re-radiated from the high-Z material as x-radiation which fills the enclosure. This indirect drive approach, long used in ignition studies and analyses, is currently being investigated in a series of experiments at the Omega laser in Rochester, NY.

These hot environments, or "high temperature hohlraums" (HTH), differ from convention inertial confinement (ICF) hohlraums. In particular, they are smaller, i.e., the smallest HTH targets are four times smaller in radius as well as in length than a typical ICF hohlraum shot at the Omega laser. Further, given the same amount of laser power as for a larger target, they are also hotter. The smallness of these targets requires a shorter laser pulse as well, as they fill with ablated gold-wall plasma very quickly. Ultimately such targets will be fielded on the National Ignition Facility (NIF). In fact, high temperature hohlraums are to be fielded at NIF this next fiscal year.

To provide the hottest environment possible it is necessary to maximize the laser-target coupling. Maximum laser power into the smallest possible target (the target diameter must at minimum accommodate the angled beams) enters us into a new regime of plasma physics. In this regime, the electron temperature is high (> 10 keV) as is the electron plasma density (> 0.1 the critical density for frequency-tripled light, 9×10^{21} cm^{-3}). Moreover, there is evidence of fast electrons. These conditions coupled with the high intensities present in the unsmoothed Omega beam provide a rich environment for laser-plasma interaction physics. Processes such as filamentation, deflection, crossed-beam energy transfer and laser scatter are currently being studied under such conditions.

In this paper we present simulation results which provide a basis for understanding the above-mentioned processes. In Sec. II we discuss the experiment and underlying motivating factors for analyzing the laser-target coupling. In Sec. III we present results from simulations of filamentation, deflection, and crossed beam energy transfer. Sec. IV addresses the nonlinear aspects of laser scatter in this regime. We discuss our findings and conclude in Sec. V.

II. MOTIVATION

In these experiments, nineteen unsmoothed Omega laser beams containing a total laser energy of 9 kJ are incident on a thick-walled (25 micrometers), gold can that is 400 micrometers in diameter as well as length. The laser pulse is a 1 ns "square" pulse.

The laser beams enter the can in three cones. The inner cone contains six beams which propagate at an angle of 23° to the axis of the can. The center cone is comprised of six beams which enter the can at an angle of 48°. The outer cone, propagating at an angle of 60° with respect to the can axis, contains seven beams. All beams are focused at the entrance to the can (laser entrance hole, or LEH), and are not smoothed. For this small can, a spa-

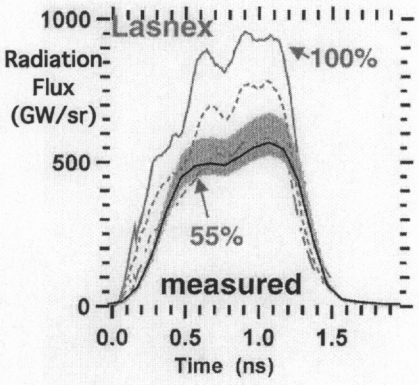

FIG. 1: A plot of radiation flux vs time. For experiment and simulation to agree, the incident power in the simulations is reduced to 55% of the power input in the experiment.

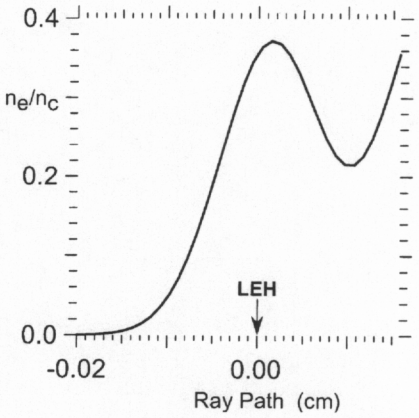

FIG. 2: The electron plasma density at $t = 350$ ps as experienced by Omega center and outer cone beams propagating into a gold can. The entrance to the can is located along the ray path at $z = 0$ cm. Negative values of z denote the region exterior to the can; positive values denote the region inside the can.

tially smoothed outer cone beam would be larger than the laser entrance hole at a 60° angle.

Fig. 1 is a plot of the radiation flux collected as a function of time at an angle of 37.4° with respect to the can axis. Shown in black is the radiation flux collected during the experiment. The grayish band surrounding the measurement depicts the uncertainty in the experimental measurement.

Simulations of these experiments were performed using the radiation-hydrodynamic code, Lasnex[3]. The simulations were post-processed to view the radiation leaving the gold can at the experimental angle of 37.4°. Shown in gray are three lines, representing simulations performed at full power, 77.5% of full power, and 55% of full power.

For experiment and simulation to agree, the incident power is reduced to 55% of that used in experiment. Moreover, 5% of the incident power was backscattered into an f/6 collection optic, the size of the incident beam. In this particular experiment, then, rad-hydro simulations cannot account for 40% of the incident energy.

It is our hypothesis that laser-plasma interactions (LPI) are responsible for this lack of energy coupling. In particular, if the beams undergo filamentation, deflection and crossed-beam energy transfer, there could be significant energy outside of the incident beams. Further, any scattering that occurs *after* deflection will miss the backscatter collection optic, as it will travel back along the deflected beam path. In the next section we summarize how filamentation, deflection, and crossed-beam energy transfer impact laser-target coupling in these reduced-scale targets.

III. THREE-DIMENSIONAL LPI SIMULATIONS

We use our massively parallel code pF3D[4] to simulate filamentation, deflection, and crossed-beam energy transfer in three dimensions (3D). In pF3D, a nonlinear hydrodynamics model of the plasma is coupled to a light wave in the paraxial approximation, which then feeds back on the plasma through the ponderomotive pressure.

Previously we have presented simulations of one outer Omega beam propagating through plasma chosen to represent those in the simulations at time $t = 450$ ps. In these simulations, there is severe filamentation, deflection, and absorption outside of the LEH. These simulations were of a size that accounted for the entire extent of the LEH as seen by a 60° Omega beam. We found that only 60% of the incident laser energy crossed the LEH plane into the target. The rest was either absorbed or deflected outside of the target.

Crossed beam energy transfer from a center cone beam to an outer beam will further reduce the laser-target coupling. This mechanism is the same as that analyzed for NIF ignition targets[2]. To quantify this reduction, we perform a pF3D simulation of two Omega beams, a center cone beam and an outer cone beam, using conditions representative of the experiment at time $t = 350$ ps.

Fig. 2 depicts the electron plasma density experienced as the beams propagate into the can. The entrance to the can (LEH) is located at $z = 0$ cm along the ray path. For values of $z > 0$ cm, the beams are inside the can, and for values of $z < 0$ cm, they are outside the can.

Fig. 3 is a plot of the electron temperature along the propagation path of the two beams at $t = 350$ ps. Everywhere along the path the electron temperature is in excess of 10 keV at this time. The LEH is again located at $z = 0$ cm.

When two beams cross in a plasma with near-sonic flow, energy can be transferred to the downstream beam when the resonance condition, $-\hat{\mathbf{k}}_{ia} \cdot \mathbf{M} = 1$ is satisfied. Here, $\hat{\mathbf{k}}_{ia}$ is the unit vector of the wavenumber associated with the ion acoustic wave given by $\mathbf{k}_{ia} \equiv \mathbf{k}_0 - \mathbf{k}_1$, where

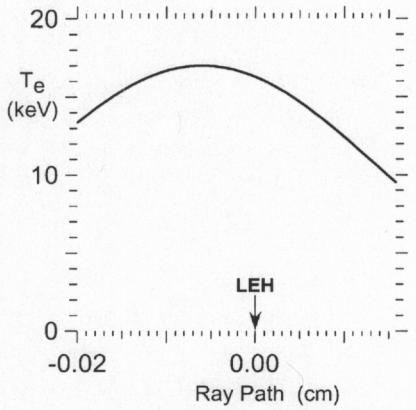

FIG. 3: The electron temperature at $t = 350$ ps as experienced by Omega center and outer cone beams propagating into a gold can. The entrance to the can is located along the ray path at $z = 0$ cm. Negative values of z denote the region exterior to the can; positive values denote the region inside the can.

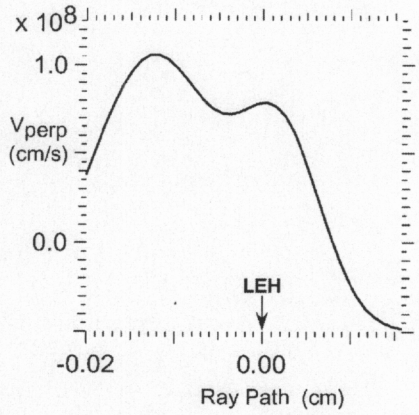

FIG. 4: The plasma transverse flow velocity at $t = 350$ ps as experienced by Omega center and outer cone beams propagating into a gold can. The entrance to the can is located along the ray path at $z = 0$ cm. Negative values of z denote the region exterior to the can; positive values denote the region inside the can. Sonic flow occurs at a speed of 9.75×10^7 cm/s.

$\mathbf{k}_0$ and $\mathbf{k}_1$ are the wavevectors of the center and outer laser beams, respectively. Also, $\mathbf{M} \equiv \mathbf{V}/C_s$, where $\mathbf{V}$ is the plasms flow and C_s is the ion acoustic speed.

Fig. 4 shows the transverse flow experienced by the center and outer beams at $t = 350$ ps. Sonic transverse flow occurs at speeds around 9.75×10^7 cm/s in this hot, gold plasma. Thus there is over 200 μm of near-sonic plasma outside the LEH of this target. We predict that resonant crossed-beam energy transfer, along with deflection and filamentation will occur.

This prediction is further supported by Fig. 5, a plot of

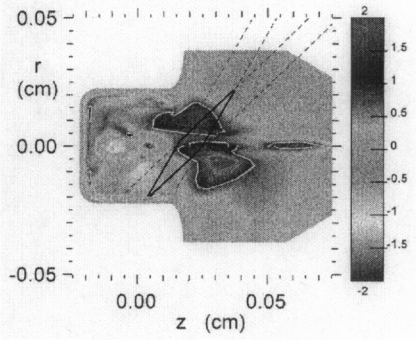

FIG. 5: A plot of the lefthand side of the resonance condition, $-\hat{\mathbf{k}}_{ia} \cdot \mathbf{M} = 1$, at 350 ps. Resonance occurs when the plotted condition is unity.

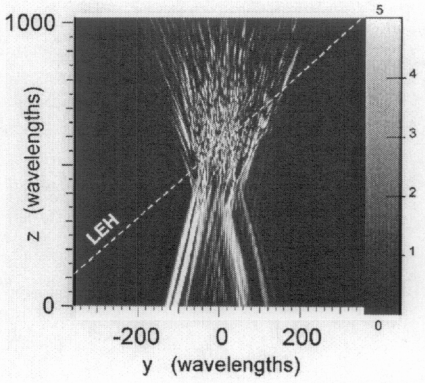

FIG. 6: A plot of the laser intensity pattern of a center and outer Omega beams after 3 ps of propagation. The lefthandmost (righthandmost) beam at $z = 0$ is the center (outer) beam. The onset of filamentation and deflection is evident.

the lefthand side of the resonance condition, $\hat{\mathbf{k}}_{ia} \cdot \mathbf{M} = 1$, at 350 ps. (Resonance occurs when the quantity plotted is unity.) The sonic surface is represented by the white contours encircling the regions of supersonic flow. Also shown in Fig. 5 is the region where the beams cross, denoted by the black diamond. The crossing region includes an extended region of near-sonic flowing plasma.

Simulation results show that resonant beam energy transfer indeed occurs under these conditions. Fig. 6 is a plot of the laser intensity pattern (far field) after just 3 ps of propagating through the above-mentioned plasma conditions. The lefthandmost beam at $z = 0$ is the center beam, and the righthandmost beam at $z = 0$ is the outer beam. The dashed white line represents the LEH plane. The onset of filamentation and deflection is evident in this plot. As time progresses, the point where filamentation and deflection occur in z moves further outside the LEH, resulting in an even larger effect.

Evidence of beam energy transfer is apparent in the near field plots. Fig. 7 is the Fourier transform of the transmitted near field $|E_k|^2$ on a plane through the center

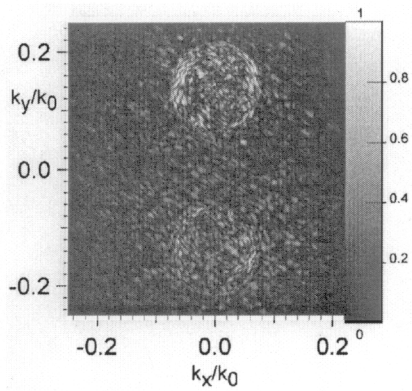

FIG. 7: A plot of the near field pattern of center and outer Omega beams after 3 ps of propagation. The bottom ($k_y < 0$) beam is the center beam, and the top ($k_y > 0$) beam is the outer beam. The onset of filamentation and deflection is evident.

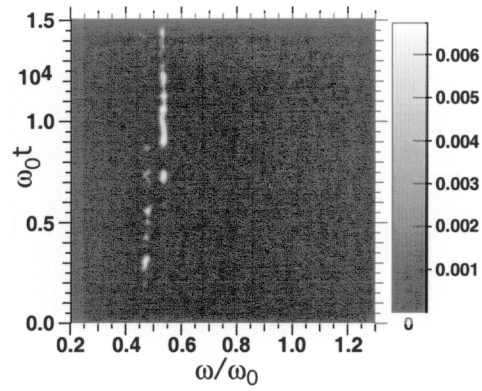

FIG. 8: A temporal streak of the backscatter for $n_e/n_c = 0.2$, $T_e = 13$ keV, and $ZT_e/T_i = 13$. The signal at $\omega/\omega_0 \sim 1.0$ is SBBS, and that at $\omega/\omega_0 \sim 0.48$ is SRBS. The signal at $\omega/\omega_0 \sim 0.53$ is stimulated Brillouin backscatter of Raman forward scatter (also occuring at $\omega/\omega \sim 0.53$, i.e., re-scatter.

of the LEH, at $z = 570$. At time $t = 0$, the near field consists of two equal amplitude f/6 beams displaced 8° from $k_y/k_0 = 0$. After 3 ps, the amplitudes of the two beams are unequal because energy has been transferred from the center beam ($k_y < 0$) to the outer beam ($k_y > 0$). Filamentation has sprayed the beams out of their original f/6 cones, filling in the near field space between the two beams. At this very early time, already 10% of the center beam energy has been transferred to the outer beam.

IV. LASER SCATTER

Laser light scattering off electron plasma waves (stimulated Raman scatter, SRS) as well as off ion acoustic waves (stimulated Brillouin scatter, SBS) can limit the laser energy coupling to the target as well. To investigate the nonlinearities associated with such mechanisms, we perform one-dimensional (1D) particle-in-cell (PIC) simulations using Zohar[5]. The plasma parameters utilized in these simulations are $n_e/n_c = 0.2$, $T_e = 14$ keV, and $ZT_e/T_i = 13$, conditions present in reduced scale targets. The laser intensity $I = 1 \times 10^{16}$ W/cm^2 is representative of an intensity slightly higher than the envelope intensity in the unsmoothed Omega beam.

Under these conditions, we find significant Raman forward scatter (SRFS), along with Raman backscatter (SRBS) and Brillouin backscatter (SBBS). For these parameters, SRFS has a growth rate comparable to that of SRBS, but is less strongly Landau damped.

Fig. 8 is a temporal streak of the laser backscatter, $\omega_0 t$ vs ω/ω_0. A value of $\omega_0 t = 1.5 \times 10^4$ is roughly 2 ps. In this figure, we see a faint signal at $\omega/\omega_0 \sim 1.0$, representing SBBS. Also present is a signal at $\omega/\omega_0 \sim 0.48$, which is SRBS. There is a third signal located at $\omega/\omega_0 \sim 0.53$, which is Brillouin backscatter of Raman forward scatter, also located at $\omega/\omega_0 \sim 0.53$.

Re-scatter of Raman forward scatter by Brillouin backscatter is not the only nonlinear process occurring. Fig. 9 is a spatial streak of the ion motion, $\omega_0 x/c$ vs $k_x c/\omega_0$. At $k_x c/\omega_0 \sim 0.6$ there is a signal representing the ion acoustic wave associated with Brillouin backscatter of the Raman forward scatter. Also present is a signal at $k_x c/\omega_0 \sim 1.2$. This is the Langmuir decay instability (LDI), where the primary electron plasma wave associated with Raman forward scatter (located at $k_x c/\omega_0 \sim 0.6$ decays into a backward electron plasma wave (at approximately the same wavenumber) and an ion acoustic wave at $k_x c/\omega_0 \sim 1.2$. For the plasma parameters, $k_{epw}\lambda_{De} \sim 0.2$ for the electron plasma wave associated with Raman forward scatter.

Both of these nonlinear mechanisms serve to limit the amplitude of the electron plasma wave associated with Raman forward scatter, and thus the amount as well as the temperature of hot electrons created by Raman forward scatter. Moreover, processes such as re-scatter further reduce laser-target energy coupling.

V. CONCLUSIONS

Laser-target coupling in reduced scale targets is a challenging endeavor. Filamentation and deflection of the outermost beams propagating into small cans occur outside the target. Simulations predict that this reduces the amount of energy on the outermost beams that enters the target by about 40%. Moreover, the center beams can transfer their energy resonantly to the outer beams via a Doppler shifted ion acoustic wave. This further reduces the amount of coupled energy.

Nonlinear laser scatter occurs given the plasma conditions and laser intensities of these experiments. Re-scatter of Raman forward scatter by Brillouin backscat-

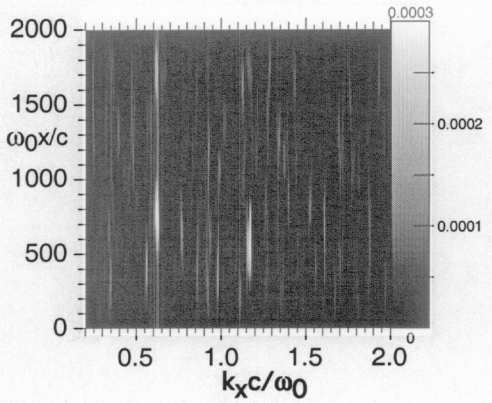

FIG. 9: A spatial streak of the ions, $\omega_0 x/c$ vs $k_x c/\omega_0$, for $n_e/n_c = 0.2$, $T_e = 13$ keV, and $ZT_e/T_i = 13$. The signal at $k_x c/\omega_0 \sim 0.6$ is the ion motion associated with SBBS of SRFS, and that at $k_x c/\omega_0 \sim 1.2$ is the ion motion associated with LDI.

ter limits the amplitude of the electron plasma wave associated with Raman forward scatter. This in turn limits the levels of forward scatter as well as the fraction and temperature of the hot electrons created via Landau damping. If the laser light were to primarily forward scatter, without undergoing re-scatter, then the scattered laser light could still couple to the target. However, if it re-scatters to backscatter, then the level of laser-target coupling will be further reduced.

Finally, the electron plasma wave associated with Raman forward scatter undergoes Langmuir decay, where it decays into a backward-propagating electron plasma wave and a forward-propagating ion acoustic wave. This mechanism limits the amplitude of the electron plasma wave associated with Raman forward scatter, and therefore restricts the amount of input laser energy into collective plasma motion.

Successful creation of a hot environment requires a full analysis of how the above processes evolve and interact with one another. A thorough investigation of the physics involved will not only help us achieve our goal, but will also further scientific understanding in this novel, high energy density regime.

VI. ACKNOWLEDGEMENTS

This work was performed under the auspices of the U.S. Department of Energy by the University of California Lawrence Livermore National Laboratory under Contract No. W-7405-ENG-48.

[1] A. B. Langdon and D. E. Hinkel, Phys. Rev. Lett. **89**, 015003 (2002).

[2] E. A. Williams, B. I. Cohen, L. Divol, M. R. Dorr, J. A. Hittinger, D. E. Hinkel, A. B. Langdon, R. K. Kirkwood, D. H. Froula, and S. H. Glenzer, "Effects of ion trapping on crossed-laser-beam stimulated Brillouin scattering", submitted to Phys. Plasmas, 2003.

[3] G. Zimmerman and W. L. Kruer, Comments Plasma Phys. Control. Fusion **2**, 85 (1975).

[4] C. H. Still *et al.*, Phys. Plasmas **7**, 2023 (2000).

[5] A. B. Langdon and B. F. Lasinski, *Methods in Computational Physics* (Academic Press, New York, 1976), Vol, 16, pp. 327-366.